AIP ADVANCES **4**, 041006 (2014)

Nuclear astrophysics in the laboratory and in the universe

A. E. Champagne,[a] C. Iliadis, and R. Longland
University of North Carolina at Chapel Hill, Chapel Hill, NC 27599-3255, USA and Triangle Universities Nuclear Laboratory, Durham, North Carolina 27708-0308, USA

(Received 4 December 2013; accepted 16 January 2014; published online 24 February 2014)

Nuclear processes drive stellar evolution and so nuclear physics, stellar models and observations together allow us to describe the inner workings of stars and their life stories. This Information on nuclear reaction rates and nuclear properties are critical ingredients in addressing most questions in astrophysics and often the nuclear database is incomplete or lacking the needed precision. Direct measurements of astrophysically-interesting reactions are necessary and the experimental focus is on improving both sensitivity and precision. In the following, we review recent results and approaches taken at the Laboratory for Experimental Nuclear Astrophysics (LENA, http://research.physics.unc.edu/project/nuclearastro/Welcome.html). © *2014 Author(s). All article content, except where otherwise noted, is licensed under a Creative Commons Attribution 3.0 Unported License.* [http://dx.doi.org/10.1063/1.4864794]

I. INTRODUCTION

Our understanding of the universe has been revolutionized by new observational technologies. Advances in detectors, computer processing power, network bandwidth, and data storage capability have enabled new sky surveys (e.g., the Sloan Digital Sky Survey), triggered many new optical transient surveys, such as the Palomar Transient Factory that probe ever-larger areas of the sky and ever-fainter sources, opening up the vast discovery space of time domain astronomy, and allowed for space missions (e.g., Kepler) that continuously monitor more than 100,000 stars. The discoveries from these surveys include revelations about stellar nucleosynthesis, unusual explosion outcomes, and remarkably complex binary star systems. The immediate future holds tremendous promise, as both the space-based survey Gaia and the ground based Large Synoptic Survey Telescope come to fruition.

Almost all questions in astrophysics ultimately require a detailed understanding of stars and stellar properties, thus challenging stellar models to become more sophisticated, quantitative and realistic in their predictive power. This in turn requires more detailed input physics, such as thermonuclear reaction rates and opacities, and concerted effort to validate models through systematic observations. Consequently, the study of nuclear reactions in the universe remains at the forefront of nuclear physics and astrophysics research. On the nuclear physics side, data on cross sections and nuclear properties of astrophysically important reactions are being obtained at radioactive ion-beam facilities and at stable-beam facilities at an accelerated pace. Radiation detectors, ion beam technology, and low-background techniques have reached an unprecedented stage of sophistication, permitting measurements of increasing precision and sensitivity. As observational astronomy has now become a quantitative science, so too has nuclear astrophysics: we recognize that insight can be gained both by acquiring new nuclear information and also by understanding the import of what remains to be measured. In the following we present our strategy, starting from an astrophysical motivation, to the identification of key reactions, to the determination of the nuclear property that

[a]Electronic address: artc@physics.unc.edu

actually needs to be measured, to laboratory measurements, to improved reaction rates that contain the new information obtained in the laboratory.

II. DIRECT MEASUREMENTS AT LENA

The reason why stars are so long-lived by our standards is that nuclear reactions at stellar temperatures are exceedingly slow, a consequence of the fact that charged particles must tunnel through the repulsive Coulomb potential in order to fuse. Thus, one of the challenges facing direct measurements of astrophysically-interesting reactions is that typical count rates are low enough that the desired signals are often indistinguishable from environmental backgrounds. This necessitates the use of high beam currents and efficient detector systems in order to boost the signal rate. Also, every important reaction represents a special case from the standpoint of measurement technique. Therefore, it is of utmost importance to have a flexible array of detectors. Experimental sensitivity can be improved by either reducing background rates or by increasing the rate of the desired nuclear reaction and a useful figure of merit is

$$F.O.M. = \frac{\text{signal rate}}{\sqrt{\text{background rate}}}. \quad (1)$$

The fact that it is inversely proportional to only the square root of the background rate seems counterintuitive at first glance, but it just reflects the fact that the precision in the residual counts is limited by the statistics of the background. Equation (1) implies that increasing beam current and thus count rate is the best way to improve sensitivity, but this is true only up to a point because there will be practical limits to how much beam a target can withstand before target degradation becomes a limitation. Consequently, background-reduction techniques must also be employed.

Environmental backgrounds can arise from natural radioactivity such as ^{40}K, ^{208}Tl, ^{238}U and its decay products, neutrons from natural fission and (α,n) reactions, and from radon gas. Gamma-rays from these sources are confined to energies below $\sim$3 MeV and can be reduced by passive shielding and by careful selection of materials used for detectors. In contrast, cosmic-ray backgrounds arising from muon-induced interactions such as direct ionization, pair-production, bremsstrahlung and nuclear interactions are much more problematic because they occur at all energies and are not significantly attenuated in passive shields. The muon flux can be reduced by going deep underground. However, beam-induced background can often be the limiting factor in the success of a measurement, which places a premium on target purity. Significant reductions in backgrounds can also be achieved by using an array of detectors in various conicidence/anticoincidence modes, as we will show below.

A. The Laboratory for Experimental Nuclear Astrophysics (LENA)

The Laboratory for Experimental Nuclear Astrophysics (LENA) was built specifically for measurements of astrophysical cross sections. As shown in Fig. 1, LENA features two accelerators: a high-intensity, low-energy accelerator based on an electron cyclotron resonance ion source (ECRIS),[1] and a 1-MV Model JN Van de Graaff accelerator. The ECRIS is mounted on a 200 kV air-insulated platform and produces high-intensity beams used to measure cross sections at energies below 220 keV. Beams from both accelerators are directed to a bending magnet used to transport them to a single target station. The ECRIS is based on the Chalk-River design,[2] which uses an input microwave frequency of 2.45 GHz and a permanent magnet to produce a roughly constant, solenoidal magnetic field of 87.5 mT within the plasma chamber. Recent improvements to the source have increased the beam current on target to 2 mA and further upgrades are in progress with the goal of increasing the beam current to 10 mA. Target stability is a concern with currents in the mA range, but the aim here is to pulse the beam with a 10% duty cycle, resulting in an average beam current of 1 mA on target, but at the same time, external backgrounds, which do not scale with the beam current, will be effectively reduced by a factor of 10. Further reductions in background can be accomplished by shielding detectors or by detection schemes that are specific to the reaction of interest, as described below. The JN accelerator has been modified with a high-power ion source and will produce beam

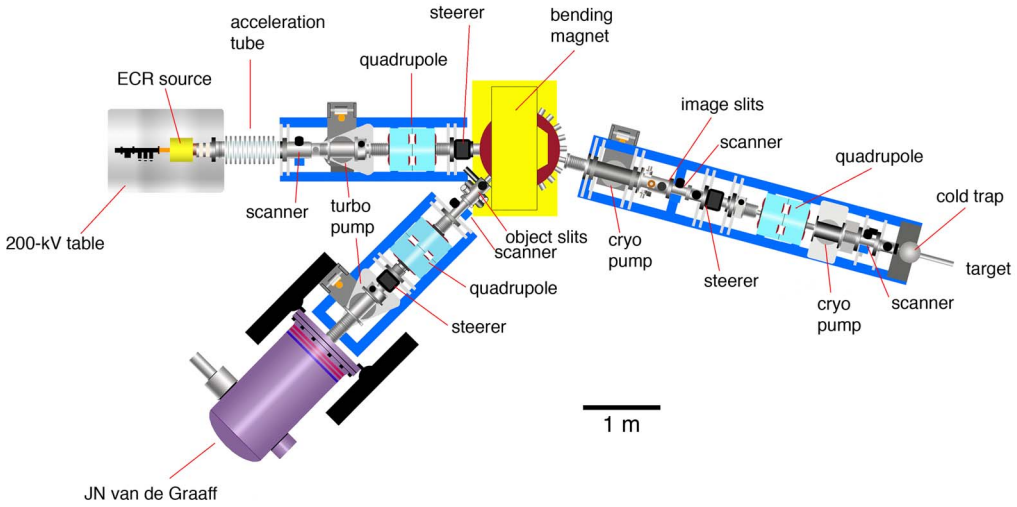

FIG. 1. Schematic layout of LENA

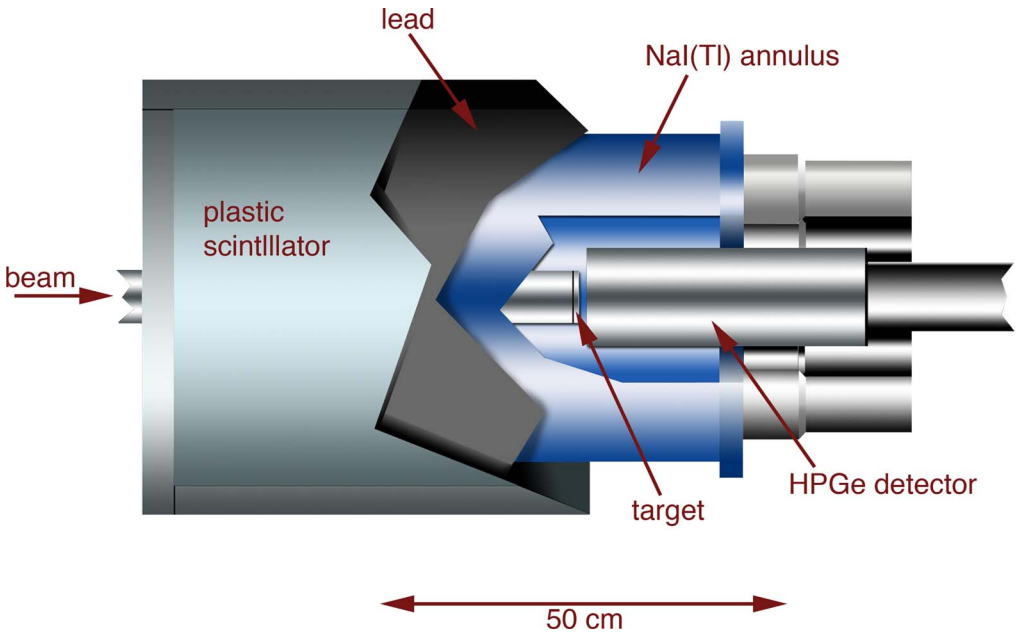

FIG. 2. HPGe-NaI(Tl) detector system used at LENA.

current on target in the range of 0.1-0.2 mA. The purpose of this accelerator is twofold: to extend measurements to higher energies, and also to test targets for composition and stability.

B. Gamma-ray detection at LENA

The basic γ-ray detection system used at LENA is described in Ref. 3 and shown in Fig. 2. Briefly, a 135% coaxial HPGe detector is centered axially on the beam line at 0° with respect to the target chamber at a distance of 1.6 cm, measured from the front of the target to the front of the detector face. The HPGe and target chamber are surrounded by an annulus of NaI(Tl) scintillators, also centered axially on the target. The detectors are surrounded on all sides by a 12.7-mm thickness of lead, which is in turn encased on all sides (except for the bottom) by 50-mm thick plastic scintillating paddles, used as a veto for cosmic-ray induced muons. The NaI(Tl) scintillator is intended to provide

a coincidence or anti coincidence condition for γ-rays detected in the HPGe detector and the energies deposited in both detectors can be combined to yield the total (detected) decay energy. Furthermore, since the annulus is optically divided into 16 elements, it can also measure the total γ-ray multiplicity in coincidence with the HPGe detector.

If the signal of interest is associated with a γ-γ cascade, then there are a number of different coincidence conditions that can be selected in order to optimize the detection sensitivity. For example, an energy (or Q-value) cut can be used to reduce backgrounds, particularly those associated with environmental sources. This is applied as

$$E_{min} < E_{Ge} + E_{NaI} < E_{max}, \tag{2}$$

where $E_{min} \sim 3$ MeV is usually sufficient to reduce room background and E_{max} is usually chosen to be the excitation energy of the populated levels in the reaction of interest. This procedure is illustrated in Fig. 3. The top part of Fig. 3 shows the 2-dimensional spectrum of NaI(Tl) vs. Ge, with a coincidence condition already applied. A gate is drawn to accept events from the reaction of interest (in this case, ^{14}N(p,γ)^{15}O), but excluding $E_{Ge} + E_{NaI} < 3$ MeV, an energy region that is dominated by room background. Events with total energies above the reaction Q-value are also excluded and these include some cosmic-ray events as well as some beam-induced background. The bottom part of Fig. 3 shows the Ge singles spectrum and the spectrum that results after the coincidence condition and 2-D gate are applied. The continuum background for $E_{Ge} < 3$ MeV is reduced by a factor of $\sim$100 beyond what is obtained with passive and active shielding. In addition, background lines are also significantly reduced, which permits the low-energy primary γ-rays to be observed. It should be pointed out that in our coincidence condition we also accept all Compton events that occur within the energy gate. Thus, the HPGe coincidence efficiency can be approximately 60% of the singles efficiency.

Detailed simulations[4] of the detection system have been performed using GEANT4,[5,6] which reproduce measurements to a high degree of accuracy. Simulations indicate that in the energy region from 600-3000 keV, about 85% of the remaining coincident background is a result of muon-induced interactions, which are reduced most efficiently by moving below ground.

C. Targets

Several considerations guide the selection of a suitable target for an experiment. Clearly, it must have a high concentration of the isotope of interest and must be able to withstand high beam currents for extended periods. However, cleanliness is also critically important because contaminants can give rise to significant beam-induced backgrounds that can be the limiting factor in experimental sensitivity. Typically, targets consist of a high dose of the isotope of interest implanted into the first few nanometers of a nickel or tantalum backing. Surface contaminants can be introduced during the manufacturing process for producing these sheets, as well as when they are machined to size. To reduce these contaminants, backings are cleaned first in an acetone bath (with agitation when needed), which remove surface oils. Wet etching in acid is then used to remove the top layer of material. Finally, the backings are outgassed by resistive heating while under vacuum. The effect of these treatment steps is illustrated in Fig. 4. Acid etching is very effective at removing carbon contamination while outgassing significantly reduces ^{19}F. Storage can also introduce contaminants and we have found that storing the targets in compressed nitrogen gas (2 atm) is preferable to storing them in vacuum.

D. What to Measure?

While it is true that our understanding of stars and stellar evolution is a central ingredient in addressing most questions in astrophysics and many in cosmology and that nuclear processes drive stellar evolution, we are usually faced with the question of determining what nuclear information is needed in order to examine a particular astrophysical problem. To illustrate the procedure that we employ, we consider the case of the radioisotope ^{26}Al. The characteristic 1809-keV γ-ray that follows the β-decay of ^{26}Al has been observed in the interstellar medium of our galaxy,[7,8] which

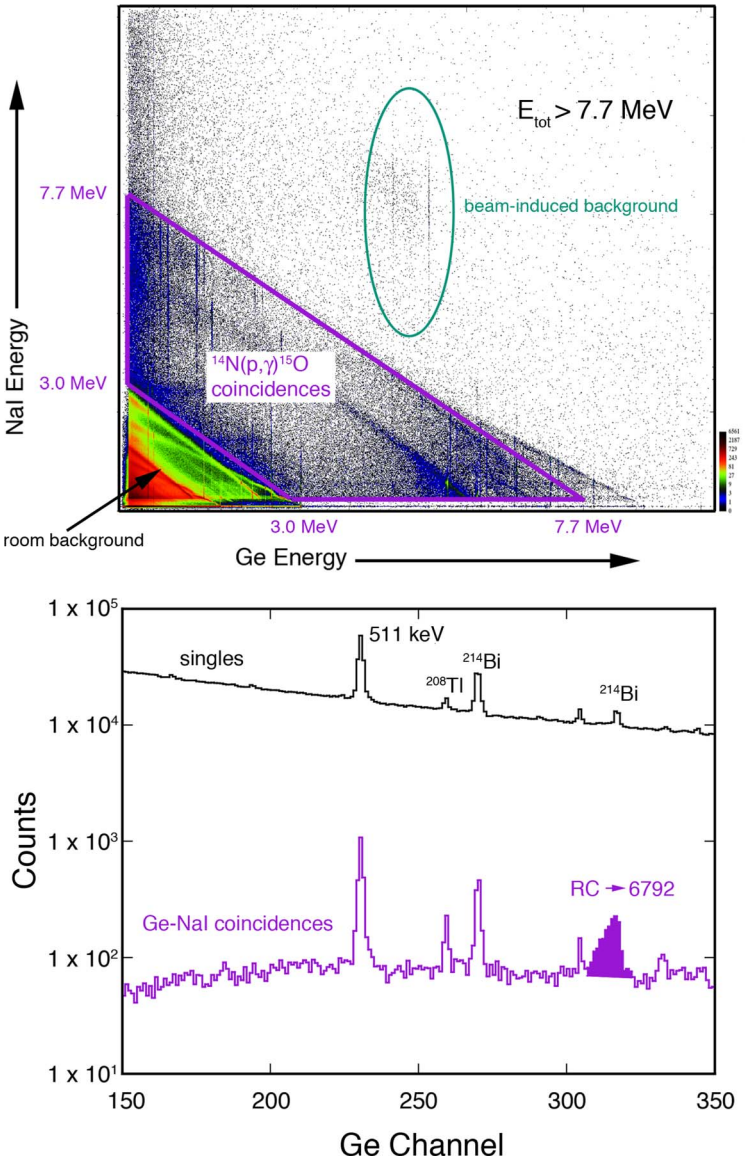

FIG. 3. Top: Illustration of HPGe-NaI(Tl) coincidence gating for ^{14}N(p,γ)^{15}O at E$_{cm}$ = 214 keV after approximately 19.3 C of accumulated charge. The gate is drawn to include all events with 3 MeV $< E_{Ge} + E_{NaI} <$ 7.7 MeV. The upper limit is near the reaction Q-value of 7511 keV. Bottom: HPGe singles spectrum (black) and HPGe-NaI(Tl) coincidence spectrum (purple). The latter results from the 2D gate drawn above. With this gate, the primary radiative-capture (RC) transition to the 6792-keV state is clearly visible whereas it is obscured by ^{214}Bi in the singles spectrum. Note that the line shape reflects the energy dependence of the cross section over the width of the target.

clearly indicates ongoing nucleosynthesis in stars. In addition, excess ^{26}Mg has been observed in meteorites and in presolar dust grains, both of which indicate the presence of a significant reservoir of ^{26}Al in the early solar system.[9–11] Asymptotic Giant Branch (AGB) stars, classical novae, Wolf-Rayet stars, and core collapse supernovae may all contribute to the ^{26}Al in both the present-day ISM and in the early solar system, but the precise source(s) remains unclear (for reviews, see[12,13]). This uncertainty goes beyond consideration of ^{26}Al as a probe of galactic nucleosynthesis since it also limits its use as a way to constrain the galactic star-formation rate.[14,15]

Determining the site of ^{26}Al synthesis involves a comparison of observations with abundance predictions from stellar models and we would like to quantify the impact of uncertainties in the nuclear database on the abundance predictions. In the context of massive stars, we start with the

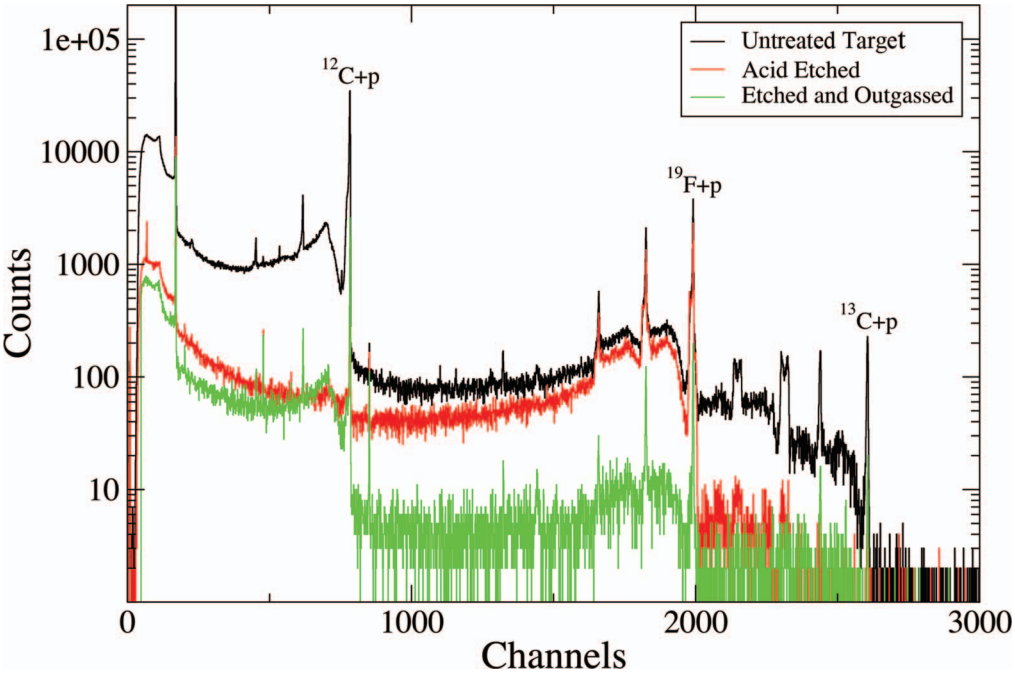

FIG. 4. HPGe spectra collected from target backings after various steps in the cleaning process. Each spectrum was taken for an accumulated beam charge of about 0.3 C at E_r(lab) = 500 keV. The detector was placed at 55° and approximately 6 cm from the target.

results of stellar models for core H-burning, convective C-shell burning and explosive Ne/C burning, sites where ^{26}Al is expected to be produced.[16] As discussed in Ref. 17, the temperature-density profiles from these calculations can be used as input in reaction-network calculations in which the rates of individual reactions are varied. The resulting changes in the final ^{26}Al abundance are an indication of what reactions are important in determining the yield of ^{26}Al – presumably the reactions that represent the focus of future measurements. While it is tempting to assume that the critical reactions are those that produce and destroy ^{26}Al, the network studies point to the importance of reactions that might otherwise be ignored. For example, in explosive Ne/C burning, the ^{26}Al abundance depends almost linearly on the rate of the ^{25}Mg(α,n)^{28}Si reaction (assuming that the ground state and the isomeric first-excited state of ^{26}Al are in thermal equilibrium).[17] The reason for this is that the (α,n) reaction reduces the reservoir of ^{25}Mg that can be converted to ^{26}Al via the ^{25}Mg(p,γ)^{26}Al. Sensitivity studies of this sort are necessary precursors to future experiments. However, as described in Sec. V, a recently-developed Monte Carlo approach can be used to quantify the sensitivity of an abundance to all of the reactions in a network, which provides more information than the brute-force technique described above.

III. RECENT RESULTS FROM LENA

A. Probing Classical Novae - Nuclear Thermometers and Mixing Meters

Classical novae are conceptually simple in the sense that the conditions that give rise to an outburst are easily described: They occur within binary systems following mass transfer from a close companion star onto the surface of a white dwarf. Matter from the underlying white dwarf is then mixed with the accreted material and after a critical temperature and density are reached, a thermonuclear runaway takes place, ejecting matter into the interstellar medium. However, unanswered fundamental questions arise when confronting the best nova models with observations: we do not seem to be able to reproduce quantitatively the detected abundance distribution; the predicted

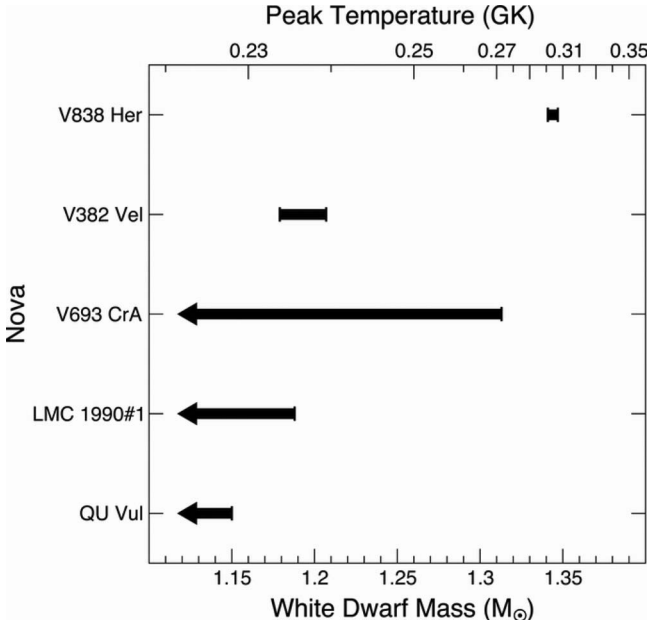

FIG. 5. Peak temperature and ONe white dwarf mass ranges derived using the nova thermometers of Ref. 19. Bracketed bars refer to white dwarf mass ranges where a definite range could be established. Bars terminating with an arrow refer to white dwarf mass ranges where only an upper limit could be determined. [Reprinted with permission from L. N. Downen, C. Iliadis, J. José, and S. Starrfield, Astrophys. J. **762**, 105 (2013), Copyright 2013 by the American Astronomical Society.]

overall ejected mass is smaller by an order of magnitude than what is deduced from observation; and the issue of why no γ-rays from novae have been detected is at present highly controversial. Obviously, nuclear reaction measurements provide a direct link between nova observables and the underlying explosion mechanism. (for a recent review, see[18]). With a better understanding of the nuclear physics input, one may reasonably hope to close these significant gaps in our understanding of thermonuclear explosions, related to mass ejection, convection, and mixing.

Observations of elemental abundances in novae ejecta could provide important constraints on several parameters that govern the outburst. We have focused on two of these, namely, *nova thermometers*, i.e. elemental ratios that are monotonic functions of peak temperature[19] and, *mixing meters*, elemental ratios that are sensitive to the degree of mixing between the accreted matter and the underlying white dwarf.[20] In principle, the sensitivity of abundances to temperature and mixing can be uncovered through detailed nova models, but only at the prohibitive cost of computing power and time. Instead, we have used a post-processing approach to perform more than 10,000 network calculations, using temperature-density profiles from 1-D hydrodynamic simulations of ONe novae, with white dwarf masses of 1.15, 1.25, 1.30 and 1.35 $M_{\odot}$. The burning zone was divided into 45 shells, each with its own T/ρ profile. Since the network calculations do not include the effects of mixing, we considered two extremes: no mixing between subshells during the explosion, and instantaneous mixing, in which the convective turnover time is faster than the nuclear burning time. In this case, each local thermonuclear rate was replaced by its mass-weighted average over the convective region. Interestingly, the geometric mean of the two extremes reproduces the elemental abundances predicted by hydrodynamic calculations to within a factor of 2 for most elements. Details of these calculations are described in Refs. 19, 20 and we briefly report on the results here.

The most useful thermometers (i.e., elemental abundance ratios with the steepest monotonic dependence on peak temperature, over the peak temperature range $T_{peak} \approx$ 200-300 MK are N/O, N/Al, O/S, S/Al, O/Na, Na/Al, O/P, and P/Al. Of these, the first 4 correspond to ratios that can be inferred from existing observations while the remaining ratios have no corresponding observations. Using this information, peak temperatures have been derived for 5 ONe novae (Fig. 5), including two (V838 Her and V382 Vel) where the observations are sufficiently precise that both the

peak temperature and white-dwarf mass could be inferred. The peak temperature for V838 Her is 0.30-0.31 MK, corresponding to a white dwarf mass of $M_{WD} = 1.34\text{-}1.35\ M_{\odot}$, while that for V382 Vel is $T_{peak} = 0.23\text{-}0.24$ GK (or $T_9 = 0.23\text{-}0.24$), which is consistent with $M_{WD} = 1.18\text{-}1.21\ M_{\odot}$. These are the only two novae where such detailed information about the explosion exists. However, it should be noted that these are model-dependent quantities and that the models assume a canonical value of 50% mixing between the accreted material and the underlying white dwarf. Thus, we have also identified elemental ratios that are rather temperature-independent, but show a strong variation with the mixing fraction. The most useful mixing meters are ΣCNO/H, Ne/H, Mg/H, Al/H, and Si/H. The ratio Na/H also satisfies the same criteria, but there are no observations of Na in nova ejecta. In almost all cases, the derived mixing fractions (defined as the percentage by mass of white-dwarf material that is mixed into the accreted matter) are on the order of 25% and significantly less that the value of 50% that is usually assumed.

It is fair to ask how these results depend on nuclear uncertainties and the effects of reaction-rate uncertainties have been evaluated using the Monte-Carlo sensitivity technique described in Sec. V. In the case of nova thermometers, the ratios O/S, S/Al, O/P, and P/Al have a pronounced temperature dependence, but are also strongly dependent on the uncertain rate of the ^{30}P(p,γ)^{31}S reaction. This reaction also affects the precision of the mixing meter Si/H. An example of the sensitivity of this ratio to variations in the ^{30}P(p,γ)^{31}S reaction rate is shown in Fig. 6.

B. The ^{18}O(p,γ)^{19}F Reaction and Presolar Grains

The ^{18}O/^{16}O ratio is very sensitive to the conditions under which the CNO cycles operate and thus, it is a very useful diagnostic of e.g., temperature and mixing. For the most part, these ratios are understood as being indicative of specific stellar environments. However, a sizable subset of presolar oxide grains, known collectively as *Group 2 grains*, exhibit a characteristic ^{18}O/^{16}O abundance ratio $\leq 1.5 \times 10^{-3}$,[23] which is at least 28% lower than the solar value, and taken to be indicative of ^{18}O depletion. This depletion may occur during the AGB phase, in what is known as *cool bottom processing* (CBP),[24] so-called because the base of the convective envelope in low-mass AGBs is cooler in comparison to what is expected for higher mass AGBs. However, temperatures during CBP are still high enough that ^{18}O can be destroyed via the ^{18}O(p,α)^{15}N and ^{18}O(p,γ)^{19}F reactions before it is mixed to the surface. As a result, grains that form in this environment will be depleted in ^{18}O.

Although, the ^{18}O(p,α)^{15}N reaction is most likely the dominant ^{18}O destruction path, the ^{18}O(p,γ)^{19}F rate may be increased by through an unobserved, low-energy resonance at $E^R_{lab} = 95(3)$ keV.[25,26] Although this resonance exists in the (p,α) channel, it must be weak in the (p,γ) channel since direct measurements have only yielded upper limits on the resonance strength of $\omega\gamma_{p\gamma} \leq 5 \times 10^{-8}$ eV[27] and $\leq 4 \times 10^{-8}$ eV.[28] Further complicating a direct search for this resonance is the fact that there is no information about the gamma-decay scheme of the corresponding excited state in ^{19}F ($E_x = 8084$ keV). However, most states in ^{19}F decay by γ-ray cascades through the first-excited state ($E_x = 110$ keV), and all levels with known decay schemes de-excite through the second-excited state ($E_x = 197$ keV). Thus, a search for the 95-keV resonance was made by looking for γ-rays with $E_\gamma = 110$ or 197 keV.

This measurement was made using the LENA ECRIS, at an energy of $E^{lab}_p = 105$ keV and with an average beam current of 0.75 mA. The JN accelerator was used to measure the target composition and resiliency via the well known $E^{lab}_R = 151$ keV resonance. Targets consisted of tantalum backings, anodized in 99.3% enriched ^{18}O water, which produced $Ta_2{}^{18}O_5$ targets with an expected target thickness of ≈18 keV at $E^{lab}_R = 151$ keV. As is shown in Fig. 7, there is no evidence for either 110- or 197-keV γ-rays. The peak intensity upper limit for the 197-keV transition was obtained from the HPGe coincidence spectrum through a Bayesian statistical approach.[30] However, a correction factor was applied to account for the unknown branching through this transition. This was calculated using a GEANT4[5,6] simulation that used the known emission probabilities for given energy levels to predict the total number of detected γ-rays arising from the 197-keV transition for a variety of coincidence gates. A possible direct transition to the ground state was also simulated.

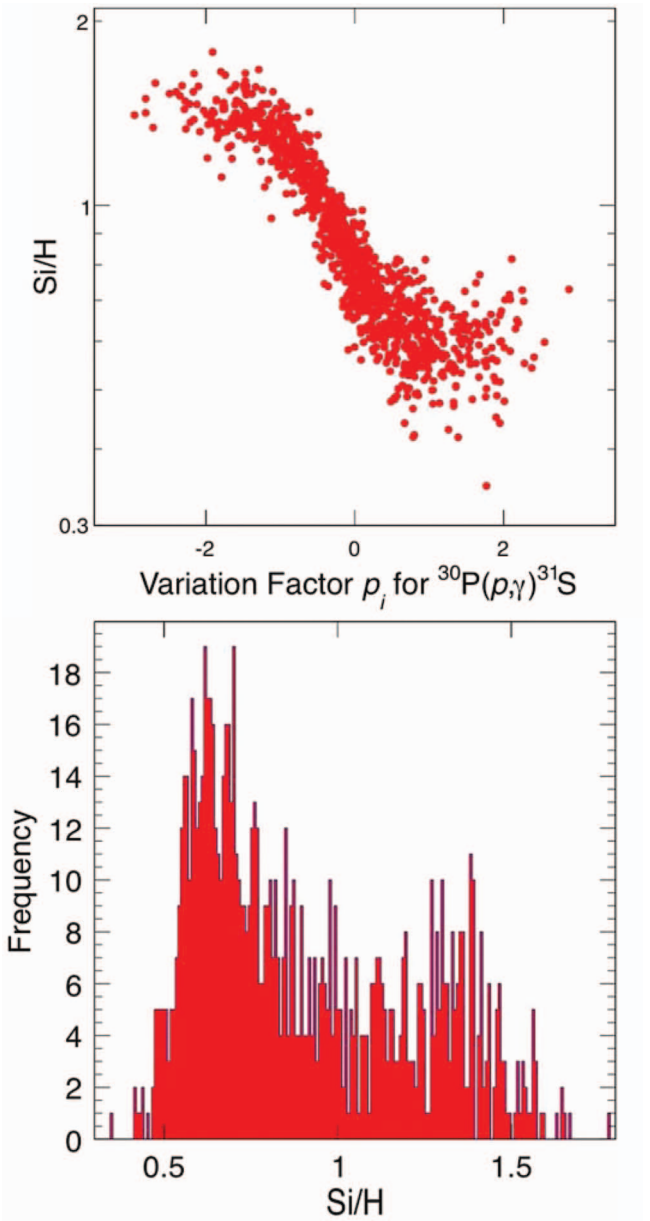

FIG. 6. Top: correlation of final elemental Si/H mass fraction ratio with the ^{30}P(p,γ)^{31}S reaction rate for a nova model for a 1.35 $M_\odot$ ONe white dwarf with 75% mixing. The variation factor, p_i is a randomly-sampled multiplier of the log-normal standard deviation for each reaction.[21,22] Details of this procedure are discussed in Sec. V B. Bottom: final elemental Si/H mass fraction ratio distribution for the same model. [Adapted with permission from K. J. Kelly, C. Iliadis, L. N. Downen, J. José, and A. Champagne, Astrophys. J. **777**, 130 (2013), Copyright 2013 by the American Astronomical Society.]

This procedure allowed us to arrive at an upper limit, $\omega\gamma_{p\gamma} \leq 7.8 \times 10^{-9}$ eV (90% CL), which is a factor of 5 below the previous result.[28] Details of this measurement can be found in Ref. 29.

This reduction in the strength of the 95-keV resonance implies that the (p,α) rate[31] exceeds the (p,γ) rate by a factor of 5,100-1,700 over the temperature range T_9 = 0.03-0.05, which is characteristic of CBP. Consequently, the (p,γ) reaction does not contribute significantly to the depletion of ^{18}O during CBP in low-mass AGB stars. As a result, the focus should now be on the ^{18}O(p,α)^{15}N reaction at low energies, where significant uncertainties are known to exist.

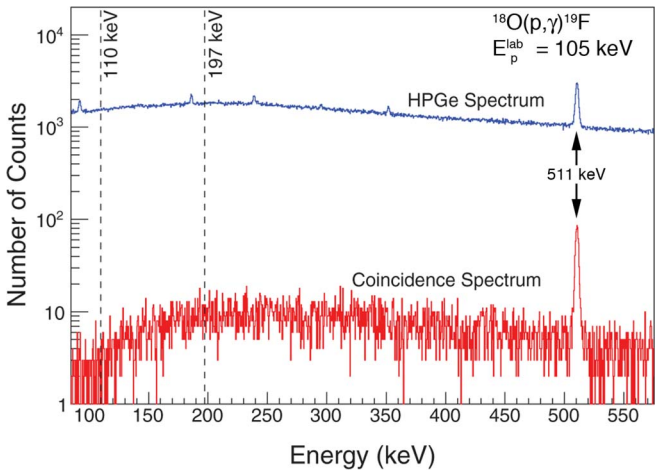

FIG. 7. HPGe singles spectrum (blue) and $\gamma\gamma$-coincidence spectrum (red). Dashed lines indicate the anticipated locations of the $1\rightarrow 0$ (110 keV) and $2 \rightarrow 0$ (197 keV) transitions in ^{19}F. The spectra shown represent on-resonance data, with a total charge accumulation of 80 C at $E_p^{lab} = 105$ keV. [Adapted from M. Q. Buckner, C. Iliadis, J. M. Cesaratto, C. Howard, T. B. Clegg, A. E. Champagne, and S. Daigle, Phys. Rev. C **86**, 065804 (2013), Copyright 2013 by the American Physical Society.]

C. The ^{23}Na(p,γ)^{24}Mg Reaction and Sodium in AGB Stars

The abundance of sodium in globular clusters is a long-standing puzzle that may reveal information about the star formation history within the cluster. Every well-studied globular cluster shows star-to-star abundance variations for light elements (C, N, O, Na, Mg and Al) with correlations between Na and Al, and O-Na and Mg-Al anticorrelations (see[32] for a review). The source(s) of these anomalous variations is currently uncertain, but possible progenitor sources include massive asymptotic giant branch (AGB) stars,[33–35] rotating, massive AGBs,[36] rotating massive stars[37,38] and massive binaries.[39] In addition, non-standard mixing may be needed to explain the observed oxygen abundances[40] as well as the O-Na anticorrelation.[41]

The ^{23}Na+p reaction plays a central role in the O-Na anticorrelation because it destroys ^{23}Na and the (p,α)/(p,γ) branching ratio determines how much material is recycled in the NeNa mass range and how much is transformed to the MgAl mass range. As was the case for the ^{18}O(p,γ)^{19}F reaction, the tabulated ^{23}Na(p,γ)^{24}Mg rate[31] showed significant uncertainties, in this case over the temperature range $T_9 = 0.04$-0.15, because of a possible, but unobserved resonance. Here, the resonance in question is located at $E_R^{lab} = 144$ keV, corresponding to a known state in ^{24}Mg at $E_x = 11831$ keV. Again, no information about the γ-decay of this state is known. Our search for this resonance followed the general procedure outlined above: On-resonance data were collected using the ECRIS at $E_p^{lab} = 147.0$ and 148.0 keV, using targets of Na_2WO_4 evaporated onto tantalum backings. These targets proved to be sufficiently stable under beam currents of 1-2 mA. States in ^{24}Mg in the vicinity of the state of interest decay primarily via γ-ray cascades, with a high fraction of the decay strength proceeding through the $1369 \rightarrow 0$ transition. Thus, this transition was used as the detection signature, but since the decay scheme is not known, a correction factor was again applied to account for the unknown branching through this transition.

A 1369-keV γ-ray was indeed observed in the HPGe detector when a 3 MeV $< E_{Ge} + E_{NaI} <$ 12 MeV coincidence requirement with the NaI(Tl) annulus was imposed, but this peak, along with another at 2754 keV (corresponding to the $2 \rightarrow 1$ transition in ^{24}Mg) also appeared in background and off-resonance spectra. We attribute them to the capture of cosmogenic neutrons by ^{23}Na in the NaI(Tl) detector. The subsequent β-decay of ^{24}Na ($T_{1/2} = 14.997(12)$ h, $Q_\beta = 5515.45(8)$ MeV[42]) primarily populates the $E_x = 4123$ keV second-excited state of ^{24}Mg, which γ-decays to the first excited state, leading to the two γ-rays that were observed. However, the coincidence scheme allows us to exclude total decay energies for the Q-value of this β-decay. In fact, a requirement of 5 MeV $< E_{Ge} + E_{NaI} <$ 12 MeV was sufficient to reduce the contribution of ^{24}Na to a negligible level. This is

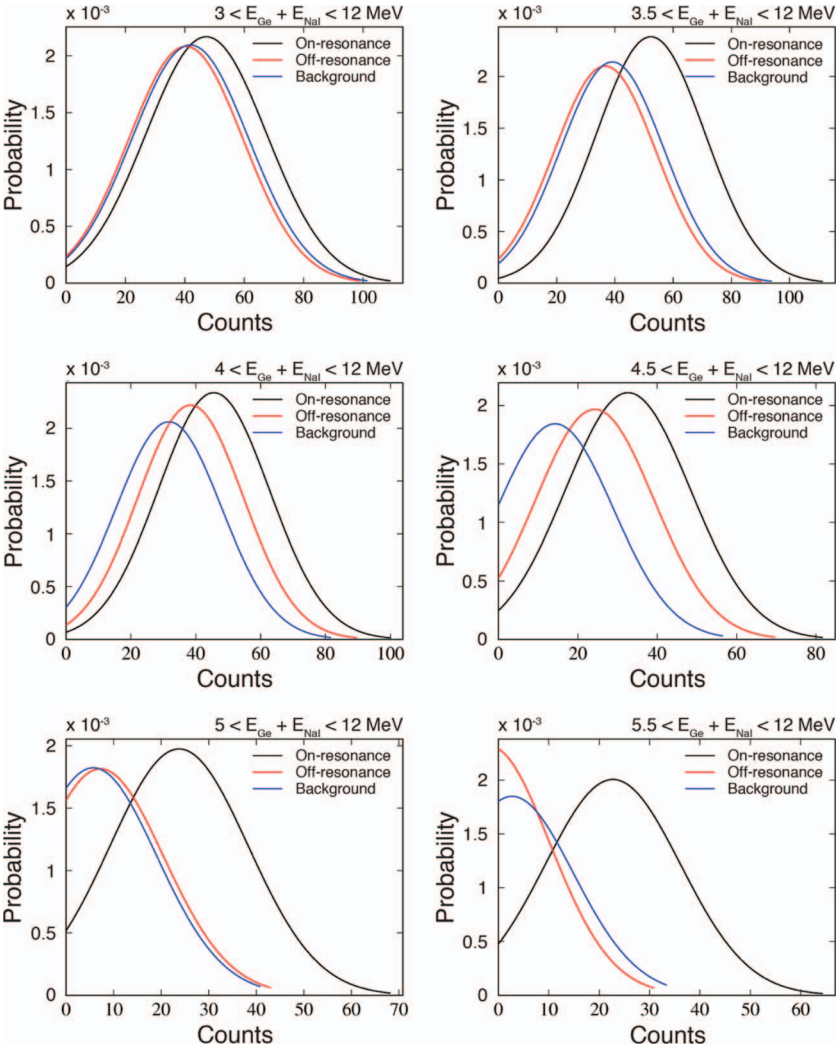

FIG. 8. Bayesean posterior distributions for the net signal intensity at $E_\gamma = 1369$ keV. Each plot was obtained for a particular coincidence energy gate for on-resonance, off-resonance, and background data subsets in black, red, and blue, respectively, using the same background and signal regions for each spectrum. With a 3 MeV $< E_{Ge} + E_{NaI} <$ 12 MeV gate, all data sets show a peak, arising from the β-decay of ^{24}Na. As the lower boundary of the coincidence gate is increased, the off-resonance and background posterior distributions become more consistent with zero, but the on-resonance distribution remains removed from zero, which is indicative of the $E_R^{lab} = 144$ keV resonance in ^{23}Na(p,γ)^{24}Mg. With a 5 MeV $< E_{Ge} + E_{NaI} <$ 12 MeV gate, the contribution from the ^{24}Na is effectively removed. [Adapted from J. M. Cesaratto, A. E. Champagne, M. Q. Buckner, T. B. Clegg, S. Daigle, C. Howard, C. Iliadis, R. Longland, J. R. Newton, and B. M. Oginni, Phys. Rev. C **88**, 065806 (2013), Copyright 2013 by the American Physical Society.]

illustrated in Fig. 8. With this coincidence cut, the mean number of counts for the on-resonance data are greater than zero, implying a residual resonance signal. However, this signal is only significant at the 1.8-σ level and therefore, we treat this result as an upper limit at the 95% CL.

The resulting resonance strength is $\omega\gamma \leq 5.17 \times 10^{-9}$ eV, a reduction of the previous upper limit[44] by a factor of 29. As a consequence, the NeNa cycle is essentially closed for temperatures below about $T_9 = 0.1$ and thus is decoupled from the MgAl region. Monte-Carlo nucleosynthesis calculations (described in Sec. V B) indicate that the ^{20}Ne(p,γ)^{21}Na, ^{23}Na(p,α)^{20}Ne, and ^{22}Na(p,γ)^{23}Mg reactions impact the O-Na anomaly in globular clusters and that the ^{23}Na(p,γ)^{24}Mg reaction now has a negligible influence on the abundance of ^{23}Na for temperatures characteristic of AGB stars. Further details of this work can be found in Ref. 43.

IV. MONTE-CARLO BASED REACTION RATES

Experimental thermonuclear reaction rates, based on nuclear physics input gathered from laboratory measurements, were first presented by Willy Fowler and collaborators more than 40 years ago ([45]and references therein). Those reaction rates were directly based on nuclear physics experiments and were distinct from reaction rates derived from theory (e.g., the Hauser-Feshbach model). The incorporation of Fowler's rates into stellar models represented a paradigm shift in astrophysics. With a solid nuclear physics foundation, stellar simulations could provide reasonable estimates of nuclear energy generation and nucleosynthesis. Subsequent work, e.g.,[46,47] incorporated newly measured nuclear physics data, but the reaction rates were still computed using techniques developed prior to 1988.

The main problem with these and more recently published thermonuclear reaction rates is that either only a single reaction rate value, without any uncertainty estimate, is reported at a given temperature, or that a recommended rate is presented together with an "upper" and "lower limit". The uncertainties, expressed as upper and lower rate limits, are frequently obtained simply by inclusion or exclusion of unobserved low-energy resonances. Such reaction rates have a major drawback since they have no rigorous statistical meaning. Specifically, since the reaction rate probability density function remains unknown, the reported rate limits cannot be quantified in terms of a coverage probability. A major obstacle in this regard was the fact that thermonuclear reaction rates are highly complex quantities derived from a multitude of nuclear properties painstakingly extracted from laboratory measurements (resonance energies and strengths, non-resonant cross sections, spectroscopic factors, etc.).

A. A New Method

A solution to this long-standing problem was devised recently, resulting in a new approach to thermonuclear reaction rates.[31,48–50] The method is conceptually straightforward and follows a Monte Carlo approach. First, all of the measured nuclear physics (input) properties entering into the reaction rate calculation are randomly sampled according to their individual probability density functions. Second, the sampling is repeated many times and thus provides the Monte Carlo reaction rate (output) probability density. Third, the associated cumulative distribution is determined and then used to derive reaction rates with a precise statistical meaning (i.e., a quantifiable coverage probability), including uncertainties. For example, for a coverage probability of 68%, the low, recommended, and high Monte Carlo rates are defined as the 16th, 50th, and 84th percentile, respectively, of the cumulative reaction rate distribution. The main challenge is to randomly sample all nuclear physics input parameters, including resonance energies and strengths, partial widths, reduced widths, astrophysical S-factors, etc., according to physically motivated probability density functions.

Depending on the nature of the nuclear physics observable, the (input) probability densities should be chosen according to the central limit theorem of statistics. It states that the *sum* of n independent continuous random variables x_i with means μ_i and standard deviations σ_i becomes a Gaussian random variable in the limit of $n \rightarrow \infty$, independent of the form of the individual probability density functions of the x_i. Many measurement uncertainties are treated as Gaussian random variables if it can be assumed that the total uncertainty is given by the *sum* of a large number of small contributions. This is usually the case for measured resonance energies, with contributions from the beam energy calibration, the measured yields, the fitting of the yield curve to find the 50% point, target inhomogeneities, dead layers, etc.

It also follows directly from the central limit theorem that a random variable will be distributed according to a lognormal density function if it is determined by the *product* of many factors. This is usually the case for measured resonance strengths (i.e., integrated resonance cross sections), which are determined from the measured number of counts of a thick-target yield, the integrated beam charge, a detector efficiency, a stopping power, etc. The lognormal distribution is given by

$$f(x) = \frac{1}{\sigma\sqrt{2\pi}}\frac{1}{x}e^{-(\ln x-\mu)^2/(2\sigma^2)} \quad (3)$$

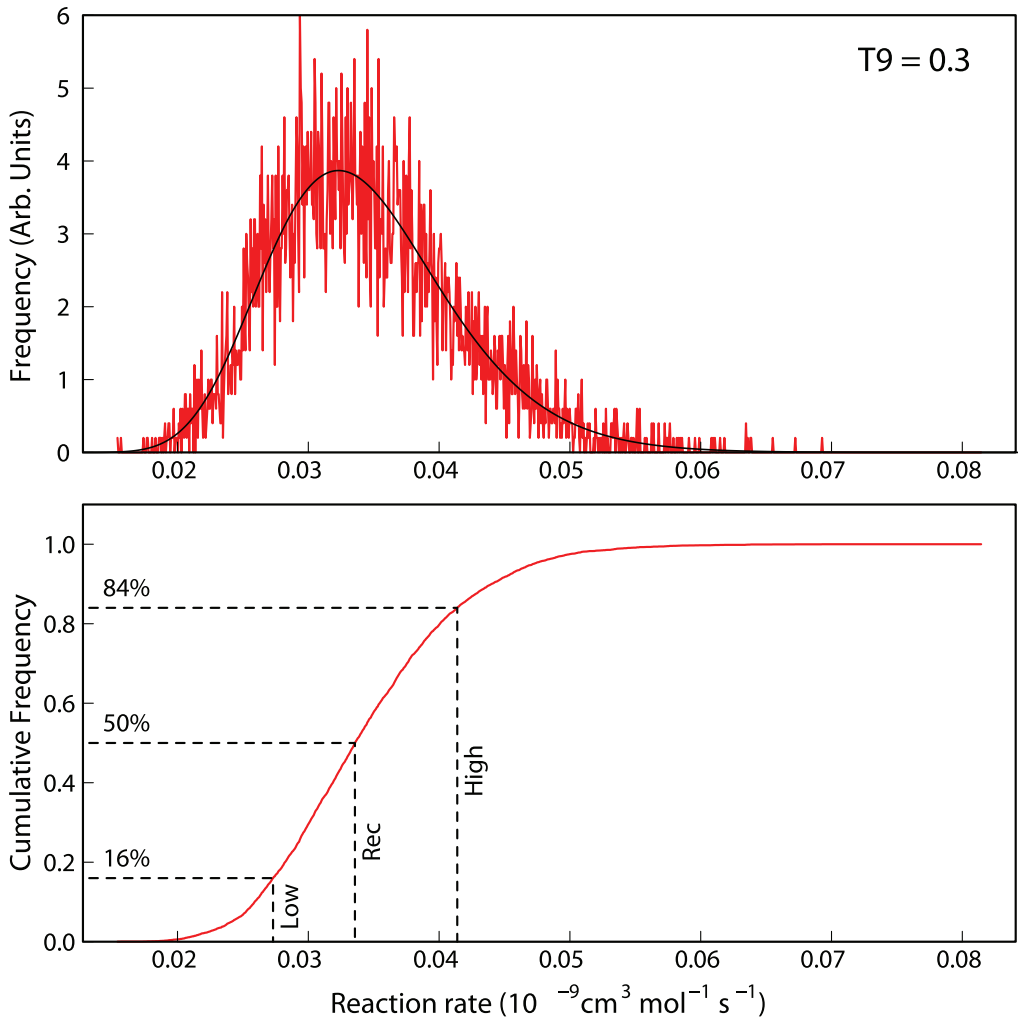

FIG. 9. Experimental Monte Carlo-based reaction rates for the crucial ^{22}Ne(α,n)^{25}Mg neutron source in the s-process at a temperature of 300 MK. The reaction rate is sampled 10,000 times. (Top) Reaction rate probability density function, shown in red; the black solid line represents a lognormal approximation, which is directly obtained from the mean and variance of the Monte Carlo rate samples (i.e., no fitting is involved). (Bottom) Cumulative reaction rate distribution; notice the much reduced scatter. The vertical dotted lines represent the low, median and high Monte Carlo reaction rates, which are obtained from the 16th, 50th and 84th percentiles, respectively.

and is defined by the two parameters μ and σ. The first determines the location of the distribution, while the second controls the width. An exhaustive account of this method can be found in Longland *et al.*[48]

As an example, we show in Fig. 9 the Monte Carlo based rates of the ^{22}Ne(α,n)^{25}Mg reaction, which is a key neutron source for the astrophysical s-process that occurs both in AGB stars and massive helium burning stars. The upper and lower panels display the Monte Carlo probability density function and the associated cumulative distribution, respectively, of the *experimental* rate at a stellar temperature of 300 MK. The 16th, 50th, and 84th percentiles, indicated in the lower part, define one particular (but arbitrary) choice for the reaction rate uncertainty, corresponding to a coverage probability of 68%. The Monte Carlo based rate of this reaction differs significantly from all previously published results. For details, see Longland *et al.*[51] It is also apparent that the Monte Carlo probability density is a smoothly varying function, without any sharp boundaries. Therefore, an "upper limit" or "lower limit" of a reaction rate, as frequently assumed in the literature, has no statistical meaning.

It is apparent that in this particular case the rate probability density can be approximated by a lognormal distribution, shown as the black solid line in the top panel. In fact, we find that this is the case for the majority of reaction rates at most stellar temperatures of interest. A detailed discussion of this issue is presented in Iliadis *et al.*[49] We will return to this point below, which is crucial for how to use the new Monte Carlo based reaction rates in nucleosynthesis studies.

B. Upper Limits of Nuclear Physics Input Parameters

Many reaction rates have contributions from unobserved low-energy resonances. More precisely, levels are known to exist near the projectile threshold energy, but the corresponding resonances have not been observed directly in the laboratory yet. At low bombarding energies, proton or α-particle partial widths are dominated in magnitude by the transmission through the Coulomb barrier and thus are usually much smaller compared to γ-ray partial widths. For example, in the simple case of a low energy resonance with only one particle channel and the γ-ray channel open, the resonance strength that enters into the calculation of the reaction rate is given by

$$\omega\gamma \equiv \omega\frac{\Gamma_x\Gamma_\gamma}{\Gamma} \approx \omega\Gamma_x = 2\frac{\omega\hbar^2}{\mu R^2}P_\ell\theta_x^2 \tag{4}$$

with Γ_x, Γ_γ, Γ the particle partial width, γ-ray partial width, and total width, respectively; μ, R, P_ℓ, and θ_x^2 denote the reduced mass, channel (nuclear) radius, penetration factor, and dimensionless reduced width, respectively; furthermore, $\omega \equiv (2J_r + 1)/[(2j_p + 1)(2j_t + 1)]$, where J_r, j_t, j_p are the spins of the resonance, target, and projectile, respectively. In simple terms, the penetration factor represents the nuclear exterior and can be computed from numerical values of Coulomb wave functions. The only unknown quantity in the above expression, assuming that J^π is known, is the dimensionless reduced width, which represents the nuclear interior.[b] The question now arises of how to implement such contributions into the Monte Carlo sampling procedure if only an upper limit for θ_x^2 is available, for example, either from experiment or from theory.

A solution to this problem is closely related to fundamental predictions of random matrix theory. The basic assumption is that energy levels in atomic nuclei at several MeV excitation energies represent chaotic systems. The reduced width amplitude for formation or decay of an excited compound nucleus is assumed to be a random variable, with many small contributions from different parts of configuration space. If the contributing nuclear matrix elements are random in magnitude and sign, then the reduced width amplitude is represented by a Gaussian probability density centered at zero, according to the central limit theorem of statistics. Consequently, the corresponding reduced width, i.e., the square of the amplitude, is described by a chi-squared probability density with one degree of freedom,

$$g(\theta^2) = \frac{1}{\sqrt{2\pi\theta^2\langle\theta^2\rangle}}e^{-\frac{\theta^2}{2\langle\theta^2\rangle}} \tag{5}$$

with $\langle\theta^2\rangle$ the local mean value of the dimensionless reduced width. This expressions is known as the Porter-Thomas distribution.[53] It implies that the reduced widths for a single reaction channel, i.e., for a given nucleus and set of quantum numbers, vary by several orders of magnitude, with a higher probability for smaller values of the reduced width. Until recently this fundamental prediction of random matrix theory had been disregarded in nuclear astrophysics. It was shown in Iliadis *et al.*[31,49] that a proper treatment of the contributions from unobserved resonances, based on the Porter-Thomas distribution, can change the estimated total thermonuclear reaction rate by orders of magnitude compared to previous predictions.

The crucial ingredient for the Monte Carlo sampling of an upper limit contribution according to the Porter-Thomas distribution is the mean value of the reduced width, $\langle\theta^2\rangle$. It is not predicted by random matrix theory, but can be obtained from the analysis of laboratory data or from a suitable

[b]The dimensionless reduced width is closely related to the spectroscopic factor, see Iliadis.[52]

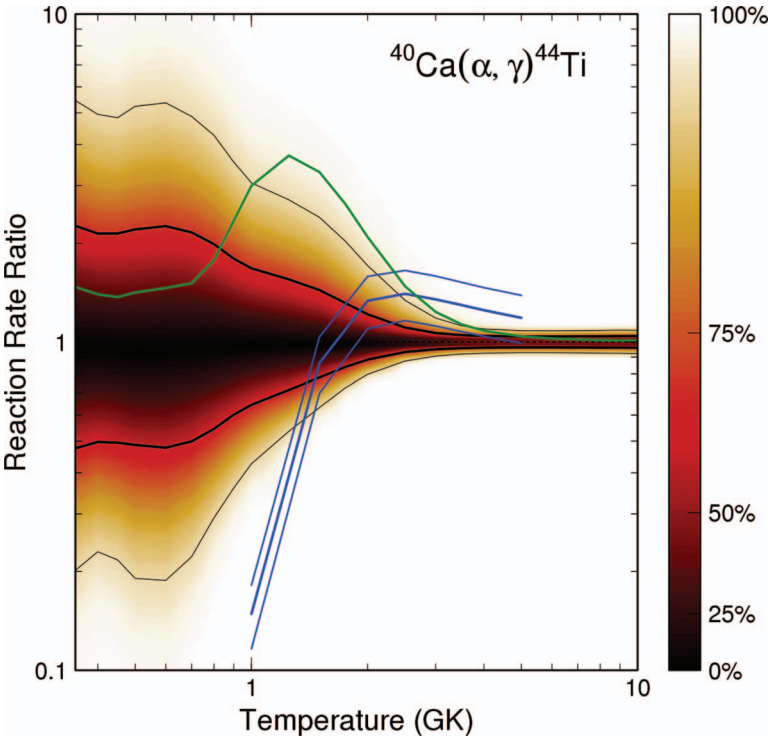

FIG. 10. Monte Carlo-based reaction rates of ^{40}Ca(α,γ)^{44}Ti. For a better comparison, all rates are normalized to the recommended Monte Carlo rate. The color-shading indicates the coverage probability in percent. The thick (thin) black lines indicate the high (low) Monte Carlo rates for a coverage probability of 68% (95%). Note that the Monte Carlo rate has no sharp bounderies (i.e., no "lower" or "upper limits"), but instead is represented by smoothly varying probability density functions along the ordinate. The blue and green lines show the rates using conventional (i.e., pre-Monte Carlo) methods. [Adapted from I. Pogrebnyak, C. Howard, C. Iliadis, R. Longland, and G. E. Mitchell, Phys. Rev. C **88**, 015808 (2013), Copyright 2013 by the American Physical Society.]

nuclear reaction model.[c] A first step in this regard was the recent extraction of mean reduced widths from high-resolution data measured at TUNL for target nuclei in the $A = 28-40$ (α-particles) and $A = 34-67$ (protons) mass ranges.[54] For example, a mean value of $\langle\theta_\alpha^2\rangle = 0.018$, averaged over target nuclei, spin-parities, and excitation energies, was obtained for α-particles, almost a factor of two larger than the preliminary value suggested in Longland *et al.*[48]

An example for the relevance of these results is given in Fig. 10. The calculated experimental Monte Carlo-based ^{40}Ca(α,γ)^{44}Ti reaction rates are shown as a contour plot (black-red-yellow; see legend on the right), where the colors signify the coverage probability between any given rate boundaries. For a better comparison, all rates are normalized to the recommended Monte Carlo rate. For example, the thick (thin) black lines indicate the high and low Monte Carlo rates for a coverage probability of 68% (95%). The blue and green lines show the rates obtained using conventional (i.e., pre-Monte Carlo) methods: (blue) previous rates,[55] where the unobserved low-energy resonances were disregarded; (green) upper limit obtained if the maximum contribution of the unobserved resonance at $E_\alpha^{c.m.} = 2373$ keV is adopted. It is obvious that the new Monte Carlo rates are significantly different from previous results. The ^{40}Ca(α,γ)^{44}Ti reaction is crucial for the production of the γ-ray emitter ^{44}Ti in core-collapse supernovae and, therefore, we are planning to explore these new rates with new stellar model calculations in the near future.

[c]The mean reduced width is related to the strength function of channel c via $s_c^J \equiv \langle\gamma_{\lambda c}^2\rangle / D^J$, where D^J is the mean energy spacing for compound levels of spin J; the reduced width, γ^2, and dimensionless reduced width, θ^2, are related by $\gamma^2 \equiv (\hbar^2/(\mu R^2))\theta^2$, with μ the reduced mass and R the channel radius. The strength function is determined by the transmission coefficient, which is key for estimating average nuclear reaction cross sections.

So far, the only systematic analysis of mean values for dimensionless reduced widths is presented in Pogrebnyak *et al.*[54] As already mentioned, these values were extracted from the available experimental data, both for protons and α-particles, for a range of compound nuclei, A, spin-parities, J^π, and excitation energies, E_x. However, the experimental values cover only a small part of the A-J^π-E_x parameter space and it is clearly desirable to have access to $\langle\theta^2\rangle$ values for all cases of interest. Considering that the data analyzed in Pogrebnyak *et al.*[54] were accumulated over a period of more than 40 years at the now decommissioned 3-MeV Van de Graaff accelerator laboratory at TUNL, it is clear that the desired $\langle\theta^2\rangle$ values need to be obtained from nuclear theory, perhaps using the shell model. More work is needed in this regard for the future.

C. Nuclear Contributions to the Total Reaction Rate

Suppose a given nuclear reaction has been identified as a key process for some astrophysical environment and that an experimentalist intends to measure this reaction. The immediate questions at hand are: which energy range should be covered in the laboratory? And which nuclear properties should in fact be measured? The usual approach is to determine first the temperature range of astrophysical interest, then to convert the temperatures to a range of bombarding energies with the help of the Gamow peak, and then address this energy region by direct or indirect measurements.[56] There are pitfalls associated with using the Gamow peak concept, as pointed out by Newton *et al.*[57] (see also later work by Rauscher[58]). In any case, this procedure can only be regarded as a rough estimate, because previously published reaction rates have no rigorous statistical meaning. For this reason, it is difficult to disentangle the impact of different nuclear physics input parameters (resonance energies, strengths, partial widths, spectroscopic factors, etc.) and their associated uncertainties on the total reaction rate.

The availability of Monte Carlo based reaction rates opens a new window of opportunity in this regard. Since each nuclear physics input parameter is sampled according to a physically motivated probability density function,[48] the Monte Carlo sampling provides a statistically rigorous coverage probability for each contribution. As an example, consider Fig. 11, showing the main fractional contributions of individual observed or unobserved resonances to the total ^{30}Si(p,γ)^{31}P Monte Carlo reaction rate. This reaction is of particular interest for interpreting observed silicon isotopic ratios in presolar nova candidate grains.[59] Different colors correspond to contributions of different resonances, while the width of each band signifies a statistically rigorous coverage probability (here 68%). Inspection of the figure clearly identifies what needs to be measured in order to improve the total reaction rate estimate. For example, at typical classical nova peak temperatures near 300 MK the total rate is dominated by the uncertainties in the contributions of the 418 keV and the 483 keV resonances. The former has not been directly observed yet, while the latter has been observed, albeit with a large uncertainty in the experimental resonance strength.

Fractional reaction rate contributions, computed using the Monte Carlo method, will likely play an important role for the design of future measurements at existing or planned nuclear physics laboratories since they identify the rate contributions to be measured, as well as the degree of precision required. A computer code allowing users to calculate experimental Monte Carlo based rates is publicly available at `starlib.physics.unc.edu`.

D. STARLIB: a New Nuclear Rate Library for Stellar Modeling

Consider again Fig. 9 that was discussed above. The solid black line in the top panel represents a lognormal function that closely describes the actual Monte Carlo reaction rate probability density shown as the red histogram. It was found in Iliadis *et al.*[49] that lognormal distributions provide a useful approximation for the majority of reaction rates. This aspect is interesting because, as already noted, a lognormal function is defined by only two parameters, μ and σ. The first parameter is related to the *median rate* via $x_{med} = e^{\mu}$, while the second parameter is related to the *factor uncertainty* with respect to the median via $f.u. = e^{\sigma}$ (for a coverage probability of 68%). Therefore, by tabulating values for temperature, T, recommended rate, x_{med}, and factor uncertainty, $f.u.$, the rate probability density function can be computed easily at each temperature of interest, according to Eq. (3).

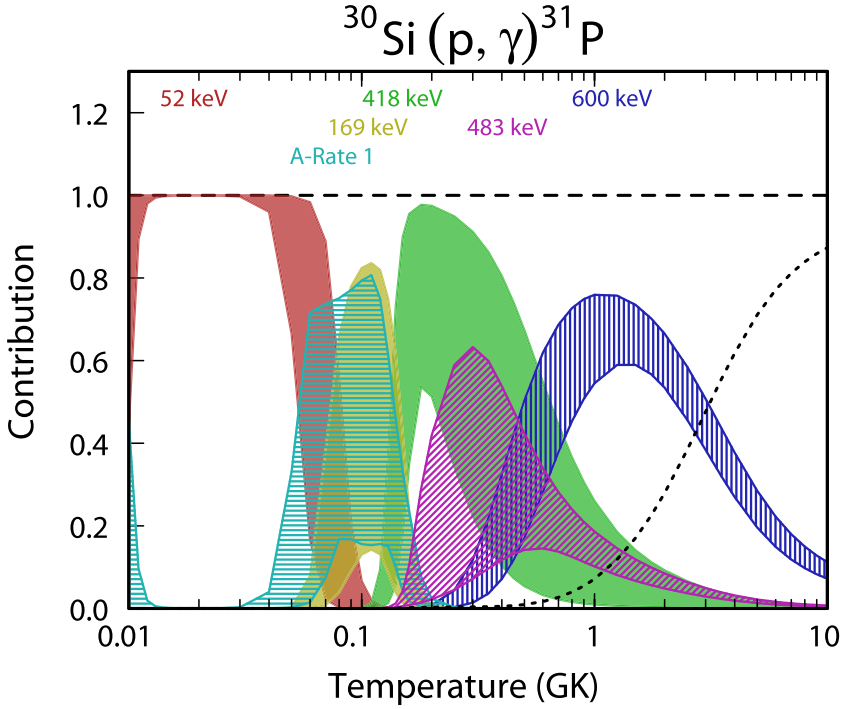

FIG. 11. Fractional contributions to the total ^{30}Si(p,γ)^{31}P reaction rate. Colors indicate different contributions. The width of a band, indicating the uncertainty of a fractional contribution, has a precise statistical meaning - a coverage probability of 68%. The results are obtained from the Monte Carlo based method. Numbers at the top denote center-of-mass energies of given resonances; "A-Rate 1" refers to the non-resonant (direct capture) rate contribution; the dotted line shows contributions of resonances with energies larger than 600 keV.

These ideas turned out to be crucial for the design of a next-generation reaction rate library, called STARLIB.[22] Existing libraries contain values of only two parameters, temperature and recommended rate, either as analytical fit formulas (e.g., JINA REACLIB[60]) or in tabular format (e.g., BRUSLIB[61]). STARLIB also has a tabular format, but contains a third parameter, the factor uncertainty, which can be used for two purposes. First, it provides an estimate for the rate uncertainty since the coverage probability for rate values between $x_{low} = e^{\mu}/e^{\sigma} = x_{med}/f.u.$ and $x_{high} = e^{\mu}e^{\sigma} = x_{med}f.u.$ amounts to 68%. Second, and more importantly, the listed values for x_{med} and $f.u.$ determine the entire rate probability density function, as was pointed out above. The latter function is obviously independent of any specific value for the coverage probability. This aspect is important because it allows for a convenient implementation of Monte Carlo based reaction rates in more realistic nucleosynthesis studies, as will be discussed in the next section. Experimental Monte Carlo based thermonuclear reaction rates are so far available for about 70 nuclear reactions involving target nuclei in the $A = 14-40$ range. Experimental β-decay rates, including their lognormal decay constant probability densities, are easily incorporated into the structure of STARLIB.[22]

A general-purpose nuclear reaction and decay library must also encompass tens of thousands of nuclear interactions for which no experimental information exists. For these reactions STARLIB contains theoretical rates that were computed using the code TALYS.[d] Reliable uncertainties for theoretical reaction rates are difficult to assess. Various claims have been made in the literature ("on average within a factor of two"), which may have been too optimistic. Previously, uncertainties have been systematically evaluated for each target and each reaction channel from the use of different sets of nuclear input models. A similar approach could be followed to estimate the uncertainties affecting the TALYS rates. However, the present version of STARLIB adopts a recommended factor of 10

[d] http://www.talys.eu.

uncertainty for any reaction rate for which no experimental cross section information exists. The factor uncertainty, together with the recommended rate, can be used to compute the lognormal rate probability density, in the same manner as for the experimental Monte Carlo rates discussed above. One of the future goals will be to replace the theoretical rates of key reactions with an experimental Monte Carlo based estimate. A detailed discussion of STARLIB can be found in.[22] The library is publicly available at `starlib.physics.unc.edu`.

V. MONTE CARLO NUCLEOSYNTHESIS STUDIES

Given the statistically meaningful Monte Carlo reaction rates presented in Sec. IV, coupled with advances in computational power, we are now in a position to explore, in detail, their effects on nucleosynthesis. Monte Carlo nucleosynthesis studies are an obvious option for investigating these effects since these methods are flexible, in the sense that all reaction rates can be varied simultaneously, or targeted groups of reactions can be studied separately. Here we will concentrate on the former case. The general strategy is to compute sample rates (as a function of temperature) for every reaction in the network and use this to compute a nucleosynthesis model. The procedure is repeated many times to build an ensemble of nucleosynthesis abundances for each nuclide. These ensembles can then be further analyzed.

Monte Carlo nucleosynthesis studies have been performed (e.g.[62–64]). However, those efforts did not utilize meaningful rate probability density functions derived from experimental nuclear physics input, but rather assigned arbitrary enhancement factors to the rates. In most cases, these enhancement factors were globally defined by identifying the type of reaction rate constraints (e.g., whether from experimental data or purely theoretical). In particular, these enhancement factors were independent of temperature. Given the discussion of Monte Carlo reaction rates in Sec. IV, it is clear that this assumptions of temperature-independence is not accurate. Rather, the rate uncertainties display a strong temperature-dependence arising from different resonant contributions. Extra steps must, therefore, be considered when reaction rates are to be varied according to a well-defined probability density function.

The best choice for performing Monte Carlo nucleosynthesis studies is to utilize directly samples obtained from the reaction rate Monte Carlo procedure. In this case, individual rate samples based on the nuclear physics input are used, thus accounting for all possible behaviors of reaction rates as a function of temperature. However, this method would require a considerable amount of effort, including detailed knowledge of all nuclear physics inputs using tools that most astrophysicists do not have access to. We, therefore, describe a reaction rate sampling method that is both simple to implement, and has been shown to agree well with more complex models.[21]

A. Reaction rate sampling method

Most reactions for which we have presented statistically meaningful uncertainties are dominated by resonances. The individual resonant contributions (in the absence of interference effects) are summed incoherently to obtain total reaction rates. Reactions that involve a large number of resonances with uncorrelated uncertainties, therefore, may exhibit complex rate variations from random sample to sample. One important constraint, however, is that these reaction rates must be smoothly varying as a function of temperature owing to the cross section convolution with the energy distribution of particles in the stellar plasma.

Recall the discussion in Secs. IV and IV D, describing how the two parameters, lognormal μ and σ, define the approximate reaction rate probability density. These parameters form the basis of our sampling scheme. By considering the properties of the lognormal distribution, we find that a single reaction rate sample, $x(T)$, at a specific temperature, T, can be represented by

$$x(T) = e^{\mu(T)} \cdot e^{p(T)\sigma(T)} \tag{6}$$

where $p(T)$ is a random variable that is normally distributed (i.e., according to a Gaussian distribution with an expectation value of 0 and standard deviation of 1). The second component of Eq. (6) represents the "uncertainty factor", which is temperature dependent. Therefore, the problem of

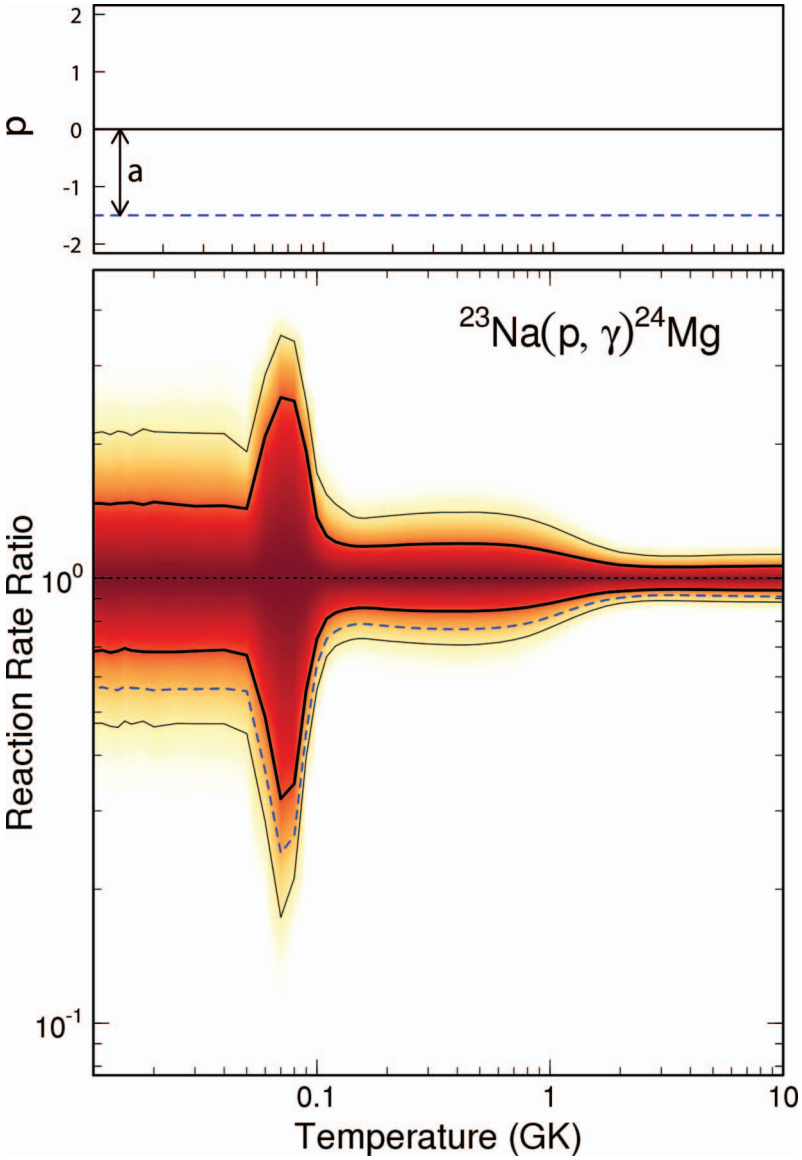

FIG. 12. Reaction rate ratio (i.e., normalized to the recommended rate) for a single rate sample of the ^{23}Na(p, γ)^{24}Mg reaction. The line at unity represents the recommended rate, while a point at 2 means that the rate is 2 times that of the recommended rate. The red density distribution represents the coverage probability of the reaction rate, with thick and thin black lines denoting the 68% and 95% uncertainties, respectively. The dashed blue line represents a single sample of the reaction rate obtained when using Eq. (6) with $p(T)$ determined according to $p(T) = a$.

sampling Monte Carlo reaction rates becomes a simple question of finding an appropriate sampling scheme for the quantity $p(T)$.

The simplest parameterization for $p(T)$ is obtained by assuming that it is independent of temperature, i.e., $p(T) = a$, where a is sampled from a normal distribution. This parameterization was found by Ref. 21 to satisfactorily reproduce the uncertainties arising from more complex sampling methods. Note that in this simplest case the uncertainty factor in Eq. (6) is still temperature dependent, and given by $e^{a\,\sigma(T)}$. This was not the case in the Monte Carlo variations of previous studies (e.g.,[64]), which essentially used a constant, temperature independent value, f, for the uncertainty factor. Figure 12 further illustrates this point, showing that a uniform value of $p(T)$ produces rates at a variety of uncertainty factors depending on the uncertainty in the rate.

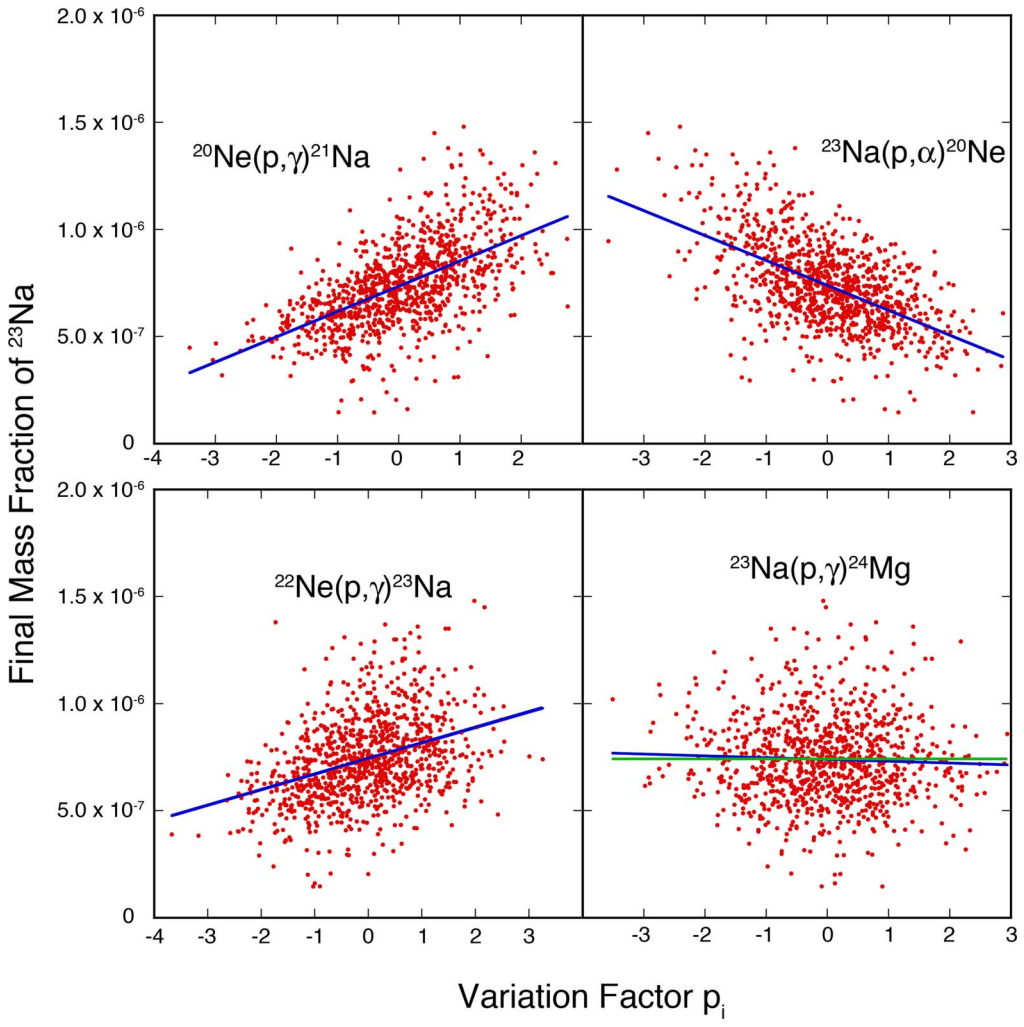

FIG. 13. Monte Carlo correlation plots showing the final ^{23}Na abundance against the variation factor, p_i. The blue lines represent linear fits to the points. In the ^{23}Na(p, γ)^{24}Mg correlation plot, the green line represents a correlation consistent with zero. [Adapted from J. M. Cesaratto, A. E. Champagne, M. Q. Buckner, T. B. Clegg, S. Daigle, C. Howard, C. Iliadis, R. Longland, J. R. Newton, and B. M. Oginni, Phys. Rev. C **88**, 065806 (2013), Copyright 2013 by the American Physical Society.]

B. Full Monte Carlo Nucleosynthesis

The role that each reaction's uncertainty plays in nucleosynthesis models can be evaluated by applying the Monte Carlo procedure discussed above to an entire reaction network. The procedure is as follows: (i) for each reaction considered, the normally distributed variables, p_i, are sampled independently; (ii) the rates obtained are used to compute the nucleosynthesis for a single post-processing network run; (iii) steps (i) and (ii) are repeated many times to obtain distributions of final nucleosynthesis abundance yields. The values of p_i are stored for each sample network run and, therefore, can be used to identify correlations between reaction rates and final abundances.

To illustrate this method, consider the ^{23}Na(p, γ)^{24}Mg reaction, described in Sec. III C. To demonstrate the power of Monte Carlo nucleosynthesis investigations, we use a temperature-density profile obtained from the base of the convective envelope in a $5M_{\odot}$, Z$\sim 10^{-3}$ AGB star model.[65] The procedure described above is applied to obtain a distribution of final abundances while storing the p_i variables for each reaction. Given this information, scatter plots can be produced to visually inspect how the abundance of ^{23}Na (or of any other nuclide) depends on the rates of particular

reactions. Numerically, we have found that the Spearman correlation coefficient is a convenient measure for identifying critical reactions (i.e., defined by strong correlations) since, unlike the Pearson coefficient, it does not rely on a linear correlation curve.

Figure 13 shows the correlations between final ^{23}Na abundance and the rates of four reactions: ^{20}Ne(p, γ)^{21}Na, ^{23}Na(p, α)^{20}Ne, ^{22}Ne(p, γ)^{23}Na, and ^{23}Na(p, γ)^{24}Mg. Note that the spread in the p_i coordinate reflects the current uncertainty for each rate. It is apparent that while the first three of these reactions exhibit correlations with the ^{23}Na abundance, the latter reaction does not. These results show that the rate uncertainties of the ^{23}Na(p, γ)^{24}Mg reaction have been sufficiently constrained by recent measurements[43] and that other reaction cross sections should now be measured in order to improve predictions of sodium abundances.

VI. OUTLOOK

Progress in nuclear astrophysics will continue to be driven by astrophysical considerations and the most important measurements will usually be the hardest to carry out. That is because by their nature, the abundances of trace elements, i.e., those with the smallest production rates at stellar temperatures, will carry the most information about the stellar environment. These can now be detected with increasing precision in stellar spectra or in meteoritic grains and these observations require improvements in the relevant nuclear physics. Direct measurements of low-energy cross sections will continue to be an important tool in these studies. These measurements can be carried out above ground in situations where the cosmic-ray background is not a limiting factor or where the reaction signature is sufficiently unique so that backgrounds can be rejected. This has driven technical developments in detectors and accelerators at LENA. Of equal importance is using new nuclear data in a quantitative way to gain astrophysical insight. Here we have described new techniques for determining reaction rates and their associated uncertainties. This combined approach of emphasizing experimental, theoretical and computational technology will continue to be the focus of the program at LENA.

ACKNOWLEDGMENTS

This work was supported in part by the US Department of Energy under contract no. DE-FG02-97ER41041 and by the National Science Foundation under award number AST-1008355, and UNC subgrant No. 201556.

[1] J. M. Cesaratto, A. E. Champagne, T. B. Clegg, M. Q. Buckner, R. Runkle, and A. Stefan, Nucl. Instrum. Meth. A **623**, 888 (2010).
[2] J. S. C. Wills, R. A. Lewis, J. Diserens, H. Schmeing, and T. Taylor, Rev. Sci. Instrum. **69**, 65 (1999).
[3] R. Longland, C. Iliadis, A. E. Champagne, C. Fox, and J. R. Newton, Nucl. Instrum. Meth. A. **566**, 452 (2006).
[4] C. Howard, C. Iliadis, and A. E. Champagne, Nucl. Instrum. Meth. A **729**, 254 (2013).
[5] S. Agostinelli *et al.*, Nucl. Instrum. Meth. A. **506**, 250 (2003).
[6] J. Allison, IEEE Trans. Nucl. Sci. **NS-53**, 270 (2006).
[7] W. Mahoney, J. Ling, A. Jacobson, and R. Lingenfelter, Astrophys. J. **262**, 742 (1982).
[8] R. Diehl, C. Dupraz, K. Bennett, H. Bloemen, W. H. J. Knoedlseder, G. Lichti, D. Morris, J. Ryan, V. Schoenfelder, H. Steinle, A. Strong, B. Swanenburg, M. Varendorff, and C. Winkler, Astron. Astrophys. **298**, 445 (1995).
[9] G. MacPherson, A. Davies, and E. Zinner, Meteoritics **30**, 365 (1995).
[10] P. Hoppe, S. Amari, E. Zinner, T. Ireland, and R. Lewis, Astrophys. J. **430**, 870 (1994).
[11] G. Huss, I. Hutcheon, and G. Wasserburg, Geochim. Cosmochim. Acta **61**, 5117 (1997).
[12] N. Prantzos and R. Diehl, Phys. Rep. **267**, 1 (1996).
[13] R. Diehl and F. X. Timmes, Pub. Astron. Soc. Pac. **110**, 637 (1998).
[14] F. X. Timmes, R. Diehl, and D. Hartmann, Astrophys. J. **479**, 760 (1997).
[15] R. Diehl *et al.*, Nature **439**, 45 (2006).
[16] M. Limongi and A. Chieffi, Astrophys. J. **647**, 483 (2006).
[17] C. Iliadis, A. E. Champagne, A. Chieffi, and M. Limongi, Astrophys. J. Suppl. **193**, 16 (2011).
[18] S. Starrfield, C. Iliadis, and W. R. Hix, in *Classical Novae*, 2nd ed., edited by M. Bode and A. Evans (Cambridge University Press, Cambridge, 2008).
[19] L. N. Downen, C. Iliadis, J. José, and S. Starrfield, Astrophys. J. **762**, 105 (2013).
[20] K. J. Kelly, C. Iliadis, L. N. Downen, J. José, and A. Champagne, Astrophys. J. **777**, 130 (2013).
[21] R. Longland, Astron. Astrophys. **548**, A30 (2012).
[22] A. L. Salaska, C. Iliadis, A. E. Champange, S. Goriely, S. Starrfield, and F. X. Timmes, Astrophys. J. Supp. **207**, 18 (2013).

[23] S. Palmerini, M. L. Cognata, S. Cristallo, and M. Busso, Astrophys. J. **729**, 3 (2011).
[24] G. J. Wasserburg, A. I. Boothroyd, and I.-J. Sackmann, Astrophys. J. Lett. **447**, L37 (1995).
[25] D. R. Tilley, H. R. Weller, C. M. Cheves, and R. M. Chasteler, Nucl. Phys. A. **595**, 1 (1995).
[26] H. W. Becker, M. Bahr, M. Berheide, L. Borucki, M. Buschmann, C. Rolfs, G. Roters, S. Schmidt, W. H. Schulte, G. E. Mitchell, and J. S. Schweitzer, Z. Phys. A **351**, 453 (1995).
[27] M. Wiescher, H. Becker, J. Görres, K.-U. Kettner, H. Trautvetter, W. Kieser, C. Rolfs, R. Azuma, K. Jackson, and J. Hammer, Nucl. Phys. A. **349**, 165 (1980).
[28] R. B. Vogelaar, T. R. Wang, S. E. Kellogg, and R. W. Kavanagh, Phys. Rev. C **42**, 753 (1980).
[29] M. Q. Buckner, C. Iliadis, J. M. Cesaratto, C. Howard, T. B. Clegg, A. E. Champagne, and S. Daigle, Phys. Rev. C **86**, 065804 (2013).
[30] Y. Zhu, Nucl. Instr. Meth. A **578**, 322 (2007).
[31] C. Iliadis, R. Longland, A. E. Champagne, and A. Coc, Nuclear Physics A **841**, 251 (2010).
[32] R. Gratton, C. Sneden, and E. Carretta, Annu. Rev. Astron. Astr. **42**, 385 (2004).
[33] P. Ventura, F. D'Antona, I. Mazzitelli, and R. Gratton, Astrophys. J. Lett. **550**, L65 (2001).
[34] F. D'Antona, V. Caloi, J. Montalbán, P. Ventura, and R. Gratton, Astron. Astrophys. **395**, 69 (2002).
[35] P. Denissenkov and F. Herwig, Astrophys. J. Lett. **590**, L99 (2003).
[36] T. Decressin and C. Charbonnel, in *IAU Symp.*, Vol. 228 (2005) p. 395.
[37] N. Prantzos and C. Charbonnel, Astron. Astrophys. **458**, 135 (2006).
[38] T. Decressin, G. Meynet, C. Charbonnel, N. Prantzos, and S. Ekström, Astronomy and Astrophysics **464**, 1029 (2007).
[39] S. de Mink, O. R. Pols, N. Langer, and R. G. Izzard, Astron. Astrophys. Lett. **507**, 1 (2009).
[40] F. D'Antona and P. Ventura, Mon. Not. R. Astron. Soc. **379**, 1431 (2007).
[41] J.-W. Lee, Mon. Not. R. Astron. Soc. **405**, L36 (2010).
[42] R. B. Firestone, Nucl. Data Sheets **108**, 2319 (2007).
[43] J. M. Cesaratto, A. E. Champagne, M. Q. Buckner, T. B. Clegg, S. Daigle, C. Howard, C. Iliadis, R. Longland, J. R. Newton, and B. M. Oginni, Phys. Rev. C **88**, 065806 (2013).
[44] C. Rowland, C. Iliadis, A. E. Champagne, C. Fox, J. José, and R. Runkle, Astrophys. J. **615**, L37 (2004).
[45] G. R. Caughlan and W. A. Fowler, Atomic Data and Nuclear Data Tables **40**, 283 (1988).
[46] C. Angulo *et al.*, Nuclear Physics A **656**, 3 (1999).
[47] C. Iliadis, J. M. D'Auria, S. Starrfield, W. J. Thompson, and M. Wiescher, Astrophys. J. Suppl. **134**, 151 (2001).
[48] R. Longland, C. Iliadis, A. E. Champagne, J. R. Newton, C. Ugalde, A. Coc, and R. Fitzgerald, Nuclear Physics A **841**, 1 (2010).
[49] C. Iliadis, R. Longland, A. E. Champagne, A. Coc, and R. Fitzgerald, Nuclear Physics A **841**, 31 (2010).
[50] C. Iliadis, R. Longland, A. E. Champagne, and A. Coc, Nuclear Physics A **841** (2010).
[51] R. Longland, C. Iliadis, and A. Karakas, Physical Review C **85**, 065809 (2012).
[52] C. Iliadis, Nuclear Physics A **618**, 166 (1997).
[53] C. E. Porter and R. Thomas, Phys. Rev., 483 (1956).
[54] I. Pogrebnyak, C. Howard, C. Iliadis, R. Longland, and G. E. Mitchell, Physical Review C **88**, 015808 (2013).
[55] D. Robertson, J. Görres, P. Collon, M. Wiescher, and H.-W. Becker, Phys. Rev. C **85**, 045810 (2012).
[56] C. Iliadis, *Nuclear Physics of Stars, by Christian Iliadis. ISBN 978-3-527-40602-9. Published by Wiley-VCH Verlag, Wenheim, Germany, 2007* (Wiley-VCH, Verlag, 2007).
[57] J. Newton, C. Iliadis, A. Champagne, A. Coc, Y. Parpottas, and C. Ugalde, Physical Review C **75** (2007).
[58] T. Rauscher, Phys. Rev. C **81**, 045807 (2010).
[59] J. Jose and M. Hernanz, Meteorit. Planet. Sci. **42**, 1135 (2007).
[60] R. H. Cyburt, A. M. Amthor, R. Ferguson, Z. Meisel, K. Smith, S. Warren, A. Heger, R. D. Hoffman, T. Rauscher, A. Sakharuk, H. Schatz, F.-K. Thielemann, and M. Wiescher, The Astrophysical Journal Supplement Series **189**, 240 (2010).
[61] M. Aikawa, M. Arnould, S. Goriely, A. Jorissen, and K. Takahashi, Astronomy & Astrophysics **441**, 1195 (2005).
[62] W. Hix, M. Smith, S. Starrfield, A. Mezzacappa, and D. Smith, Nucl. Phys. A **718**, 620 (2003).
[63] L. F. Roberts, in *International Symposium on Nuclear Astrophysics - Nuclei in the Cosmos* (2006).
[64] A. Parikh, J. José, F. Moreno, and C. Iliadis, The Astrophysical Journal Supplement Series **178**, 110 (2008).
[65] P. Ventura and F. D'Antona, Astron. Astrophys. **431**, 279 (2005).